scientific reports

Check for updates

OPEN

Reduction of absorption of Ta_2O_5 monolayers through the suppression of structural defects by employing an appropriate ionic oxygen concentration

Lin Wang[1,2], Weili Zhang[2,5]✉, Ruijin Hong[1]✉, Kun Wang[2], Menglei Wang[2], Qinmin Wang[2], Kui Yi[2,5] & Jianda Shao[2,3,4,5]

Ultralow-absorption laser films have critical applications in high-power continuous-laser and gravitational-wave-detection systems. During film deposition, the ionic oxygen concentration significantly affects the absorption loss of the film. In this study, Ta_2O_5 monolayers were deposited using an ion-assisted electron beam evaporation technique, and the weak absorption at 1064 nm, temperature rise, optical band gap, element content, and binding energy were tested and analyzed. The band structure and microdefects of the Ta_2O_5 films were characterized, and their correlation with the absorption properties was established. The analyses revealed that the primary mechanism responsible for reducing the absorption loss in Ta_2O_5 films was an appropriate ionic oxygen concentration, which improved the optical band gap and stoichiometric ratio and reduced oxygen vacancy defects. For Ta_2O_5 monolayers deposited with the optimal ionic oxygen concentration, the weak absorption was approximately 7.2 ppm and the temperature rise was approximately 0.6 °C, 1/4 and 1/3 of the values of those deposited with an excessive concentration, respectively—an important finding in the preparation of ultralow-absorption laser films.

Keywords Ion-assisted deposition (IAD), Ta_2O_5 films, Absorption loss, Ionic oxygen concentration

With the continuous development of laser technology, the absorption performance of film components within laser systems has become increasingly important. During a long period of high-power continuous laser irradiation, a weak absorption loss causes the conduction and accumulation of heat from the light energy in a film. Thus, the surface temperature of the film rises, which can cause a certain degree of melting or changes in the material characteristics and optical properties, ultimately resulting in damage to the film components. Furthermore, heat deposition from absorption can distort film components, resulting in poor beam quality. Therefore, laser films with ultralow absorption are crucial for high-power laser systems such as laser weapons[1–3], laser inertial confinement fusion (ICF) systems[4–8], and high-precision measurement systems, including gravitational wave detection[9–11] and laser gyroscope systems[12,13].

Ta_2O_5, generally deposited using electron beam evaporation, ion beam sputtering, and ion-assisted deposition (IAD)[14–20], is a high-refractive-index material commonly used in laser systems, particularly for ultrahigh reflectivity and ultralow absorption applications. Among these methods, IAD and bombarding a film with an oxygen ion beam improve the structural defects in the film and better replenish the oxygen loss of the source material, thus reducing the oxygen vacancy defects in the film, which plays an important role in decreasing its absorption loss.

[1]Engineering Research Center of Optical Instrument and System, Ministry of Education and Shanghai Key Lab of Modern Optical System, University of Shanghai for Science and Technology, No. 516 Jungong Road, Shanghai 200093, China. [2]Laboratory of Thin Film Optics, Shanghai Institute of Optics and Fine Mechanics, No. 390 Qinghe Road, Shanghai 201800, China. [3]Hangzhou Institute for Advanced Study, University of Chinese Academy of Sciences, Hangzhou 310024, China. [4]CAS Center for Excellence in Ultra-intense Laser Science, Shanghai 201800, China. [5]Key Laboratory of Materials for High Power Laser , Shanghai Institute of Optics and Fine Mechanics, No. 390 Qinghe Road, Shanghai 201800, China. ✉email: wlzhang@siom.ac.cn; rjhong@usst.edu.cn

APS O_2 flow rate (sccm)	Actual thickness (nm)
25	1448
30	1465
35	1483

Table 1. Ta_2O_5 film actual thickness.

Group	APS O_2 flow rate (sccm)	Discharge current (A)	Bias voltage (V)	Kr #1 flow rate (sccm)	Kr #2 flow rate (sccm)
A	25	50	130	2	8
B	30	50	130	2	8
C	35	50	130	2	8

Table 2. Ta_2O_5 process parameters.

The absorption loss of a film is mainly due to absorption during the deposition process, considerably influenced by process parameters such as the ion source voltage and current, oxygen flow rate, auxiliary gases, and substrate temperature. In particular, the oxygen flow rate directly affects the stoichiometric ratio of an optical oxide film. Zhang et al.[21] used an IAD method to control the absorption of Ta_2O_5 films by adjusting the oxygen flow rate and substrate temperature, which produced films with reasonable optical properties in the near-infrared region. Liu et al.[22] investigated the effects of the process parameters on the optical band gap of Ta_2O_5 films and found that the oxygen flow rate had the most effect on the forbidden bandwidth. A higher oxygen flow rate improved the forbidden bandwidth of the films—the key to preparing ultralow-loss films. Chen et al.[23] used two different molecular oxygen flows and four different ionic oxygen flows to study the effect of the ionic oxygen concentrations and oxygen flow rates on the optical properties of Ta_2O_5 films. With an increase in the ionic oxygen concentration, the refractive index first increased and then decreased. The extinction coefficient of Ta_2O_5 films with 25sccm O_2^+ were much higher than those of Ta_2O_5 films with 30, 35, and 40sccm O_2^+. The extinction coefficient of the last three groups of samples exhibited little difference. In IAD, an ion beam is emitted by ionizing pure oxygen in the ion source, known as ionic oxygen. This process significantly affects the properties of ultralow-absorption films. Although ionic oxygen can increase the oxidizing capacity and reduce the oxygen vacancy defects, bombarding films with an ion beam stream may also selectively sputter out the oxygen in the films, leading to new oxygen vacancy defects. Thus, when using different IAD processes for dielectric films, the absorption performance is not positively correlated with the oxygen concentration; hence, an optimal concentration exists, which has not been extensively studied. Thus, conducting absorption studies of films deposited with the assistance of different ion-source oxygen flow rates is necessary.

In this study, Ta_2O_5 monolayers were deposited via ion-assisted electron-beam evaporation, and the effects of the oxygen flow rate in an advanced plasma source (APS) on the absorption and structural properties of Ta_2O_5 films during deposition were investigated. The optical band-gaps of the Ta_2O_5 films deposited at different ionic oxygen concentrations were calculated using Tauc curve fitting. The O and Ta contents of the Ta_2O_5 films were determined by X-ray photoelectron spectroscopy (XPS), with the binding energies and relative contents of the adsorbed oxygen peaks obtained by fitting the elemental O split peaks. The temperature rise under continuous laser irradiation and the weak absorption at 1064 nm of the Ta_2O_5 films were tested, and a correlation with the microstructure was established. The absorption properties of the films were elucidated based on microscopic mechanisms, with the coating process optimized accordingly. Using the optimal ionic oxygen concentration parameters for film deposition can enhance the absorption performance of the films and facilitate the preparation of laser films with ultralow absorption loss in optical systems.

Experiments

Ta_2O_5 monolayers were deposited using ion-assisted electron-beam evaporation. The film samples were coated using a Syruspro1110DUV coating machine (Leybold Optics, Germany). The coating source material consisted of high-purity Ta_2O_5 solid particles, and the films were deposited on JGS1 fused silica substrates. The initial vacuum pressure used for the film deposition was approximately 9×10^{-4} Pa, while that for the coating was approximately 2×10^{-2} Pa. The substrate baking temperature was 140 °C, and the evaporation rate of the material was 0.4 nm/s. The film thickness was set to 1500 nm and was monitored using a crystal. The actual film thicknesses for the different APS oxygen flow rates were fitted by Essential Macleod 11.0 software[24] and are listed in Table 1. An Advanced Plasma Source (APS, Leybold Optics) was used as an auxiliary ion source and charged with two channels of krypton (Kr) gas as the working gas: Kr1 at a flow rate of 2 sccm and Kr2 at 8 sccm, while oxygen (O_2) with purity better than 99.999% was filled in the ion source at a flow rate varying from 25 to 35 sccm. The ion source discharge current was 50 A, and the ion source bias voltage was 130 V. Finally, the deposited films were annealed in an atmospheric environment for 12 h at an annealing temperature of 250 °C. Ionic oxygen refers to the emission of an oxygen ion beam generated when pure oxygen passes into the APS, with its concentration controlled by the oxygen flow rate through the APS. The process parameters for the different APS oxygen flow rates are listed in Table 2.

A spectrophotometer (Perkin-Elmer Lambda 1050 UV/VIS/NIR) with a resolution of 0.1 nm and measurement accuracy of 0.08% was used to test the transmission spectra of the films at an incidence of 0°. The refractive index and extinction coefficient of the film material were obtained by fitting the transmission spectral data using the envelope method[25] based on the Essential Macleod 11.0 optical design software[24]. The refractive index at either wavelength could be obtained using the Cauchy formula:

$$n(\lambda) = A + B/\lambda^2 + C/\lambda^4,$$

where n(λ) is the refractive index at the corresponding wavelength; λ is the wavelength; A, B, and C are the coefficients to be fitted. The weak absorption of the films at 1064 nm was measured using a self-made system based on the surface thermal lensing technique[26,27]. The test environment temperature was 23.5 °C, relative humidity was 35%, and the incidence angle was 0°. A total of 12 measurement points were randomly selected on the sample surface, with their average value obtained. The temperature rise of films irradiated with a continuous 1064 nm laser was measured, and the surface temperature was monitored using an infrared thermal imager before and after irradiation. The optical band gap of the films was calculated using the Tauc equation[28]:

$$E_g = h\nu - (\alpha h\nu)^{1/2}/A,$$

where h, ν, α, A, and E_g represent Planck's constant, the frequency of incident light, the absorption coefficient, the band-edge parameter, and the optical band gap, respectively. The chemical composition of the Ta_2O_5 films was analyzed using an X-ray photoelectron spectrometer (XPS, Thermo Scientific K-Alpha) equipped with a monochromated Al-Kα (energy: 1486.6 eV) X-ray source. To remove any water and oxygen adsorbed on the surface of the films, the surface was etched using 1 KeV argon ions for two cycles, each lasting 8 s, before scanning. The binding energy of the tested element was calibrated through translation based on the disparity between the binding energy values of the C1s fine spectrum and standard peak (284.8 eV)[29].

Results and discussion

Optical constants of Ta_2O_5 films

Figure 1 shows the transmission spectra of Ta_2O_5 films deposited on quartz substrates at different APS oxygen flow rates. Figure 2(a) and (b) show the refractive indices and extinction coefficients of the Ta_2O_5 films deposited at different APS oxygen flow rates, respectively. As the APS oxygen flow rate of groups A–C gradually increased, the refractive index showed a slight and insignificant decrease, while the extinction coefficient initially decreased and then increased. To visualize the correlation between the refractive index and extinction coefficient of Ta_2O_5 films and the APS oxygen flow rates, the refractive index and extinction coefficient at 532 nm were selected, and accordingly, their trends with the change of the APS oxygen flow rates were plotted, as shown in Fig. 3. The extinction coefficient of the group B samples deposited at the optimum ionic oxygen concentration was smaller than that of the group C samples deposited at a higher ionic oxygen concentration. These findings indicated that a higher ionic oxygen concentration increased the absorption of the Ta_2O_5 films.

Absorption loss and temperature rise of Ta_2O_5 films

The weak absorption values at 1064 nm in the group A–C samples were measured using the surface thermal lensing technique[26,27]. Figure 4 shows the relationship between the weak absorption at 1064 nm and the APS oxygen flow rate of the Ta_2O_5 films. The figure shows that the group B samples exhibited the smallest absorption values, lower than those for groups A and C, consistent with the extinction coefficients shown in Fig. 2(b). The absorption values of the Ta_2O_5 films decreased from 10 ppm to 7.2 ppm as the APS oxygen flow rate increased from 25 sccm to 30 sccm, and the absorption increased significantly to 31.3 ppm when the APS oxygen flow rate increased to 35 sccm. These results indicated no positive correlation exists between the absorption performance and oxygen concentration, suggesting the presence of an optimal concentration.

The surface temperature increases for the samples in groups A–C were tested using continuous laser irradiation, where the laser parameters are listed in Table 3. A thermal imaging camera was used to monitor the surface temperature distributions of the samples in groups A–C—irradiated with a laser power density of 35 kW/cm^2, as illustrated in Fig. 5. The figure clearly shows that the change in the surface temperature within the laser-irradiated region was significantly greater for group C than for groups A and B.

Figure 6 shows the temperature rise values of the samples in groups A–C irradiated with different laser power densities. When the laser power density was low, the surface temperature of the films did not change significantly; in contrast, when the laser power density increased, the surface temperature continued to increase. The samples in group C had the highest temperature increase values, followed by those in group A. The samples in group B had the lowest values, consistent with the results of weak absorption at 1064 nm shown in Fig. 4. The temperature increase reflected the heat absorption capacity of the film, where a higher temperature increase indicated a greater absorption loss. The temperature rise values of the Ta_2O_5 films irradiated using a laser power density of 35 kW/cm^2 decreased from 0.9 °C to 0.6 °C as the APS oxygen flow rate increased from 25 sccm to 30 sccm, and increased significantly to 2.0 °C when the APS oxygen flow rate increased to 35 sccm. Therefore, a higher ionic oxygen concentration increased the absorption loss of the Ta_2O_5 film.

In addition, increasing the temperature in the area of continuous laser irradiation distorted the film surface, leading to a deterioration of the beam quality. Theoretical simulations were performed using the COMSOL Multiphysics 6.0 software[30] to fully understand the thermal distortion of the group A–C samples under continuous laser irradiation. Figure 7 shows the simulated surface morphology distribution of the group A–C samples irradiated using a laser power density of 35 kW/cm^2. The figure shows that the maximum surface deformation of the samples in group C was 2.26 nm, significantly larger than the values of 0.97 and 0.46 nm for groups A and B, respectively. These results were consistent with the results of the temperature rise test. Therefore, a higher ionic oxygen concentration increased the temperature rise of the Ta_2O_5 films under continuous laser irradiation, with a higher temperature rise causing a higher absorption loss and more serious thermal distortion.

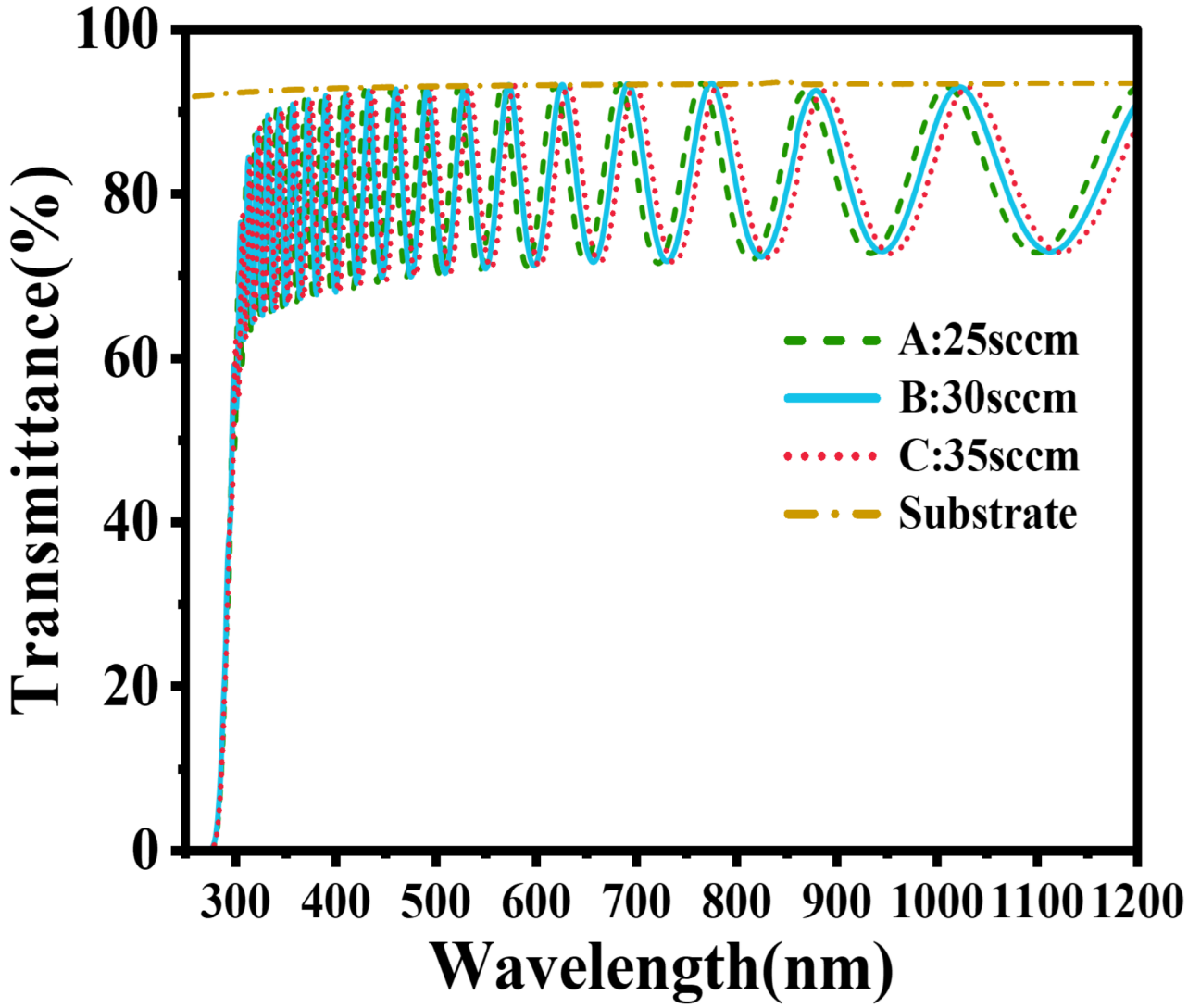

Fig. 1. Transmission spectra of Ta_2O_5 films.

Microstructure of Ta_2O_5 films

To understand the differences in the absorption losses of the Ta_2O_5 films prepared under different processing conditions, thoroughly studying the microstructure of each film, linked to the macroscopic absorption properties, was necessary. The coating process was then optimized to improve the absorption properties of the films.

XPS tests were performed on films deposited at different ionic oxygen concentrations to study the stoichiometric ratios and oxygen vacancy defects in the films. Figure 8(a)–(c) show the fine spectra of Ta 4f, where the split-peak fitting can be separated into two peaks, $4f_{5/2}$ and $4f_{7/2}$, with binding energies of approximately 28.4–28.7 eV and 26.4–26.8 eV, respectively, suggesting that the composition of the Ta in the films was mainly Ta^{5+} [31,32]. Figure 8(d)–(f) show the fine O 1s spectrum, which consists of an asymmetric Gaussian-type curve with a distinct tail toward the high-binding-energy side. Thus, the O 1s peak decomposes into two Gaussian peaks, where the lattice oxygen peak located near 531 eV corresponds to the Ta-O bond and the typical XPS peak located near 532.5 eV can be attributed to adsorbed oxygen[33]. The O/Ta ratios were obtained from the integrated areas of the two elements in the XPS spectra and the sensitivity factors. The results showed that when the APS oxygen flow rate was 30 sccm, the area percentage of the adsorbed oxygen peak of the Ta_2O_5 films was 8.93%, and the O/Ta ratio was 2.499. As the APS oxygen flow rate was increased to 35 sccm, the area percentage of the adsorbed oxygen peak of the Ta_2O_5 films increased to 9.93%, and the O/Ta ratio decreased to 2.469, indicating that an excessive ionic oxygen concentration was detrimental to the full oxidation of the films. Meanwhile, the binding energy of the adsorbed oxygen peak in the Ta_2O_5 films shifted from 532.38 to 532.48 eV as the APS oxygen flow rate increased from 30 to 35 sccm. The binding energy of the adsorbed oxygen peak shifted toward a higher binding energy[33–35], suggesting an increased presence of oxygen vacancies at higher APS oxygen flow rates. More oxygen vacancy defects created defect energy levels in the forbidden band, leading to an increase in the absorption loss of the film; therefore, the ionic oxygen concentration could not be excessively increased.

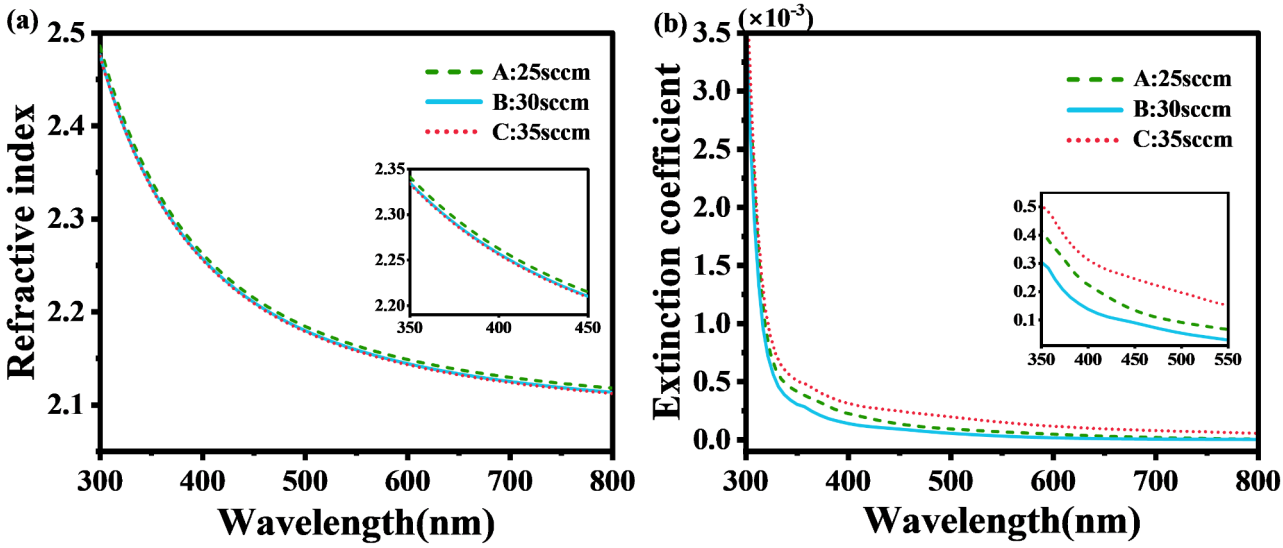

Fig. 2. Optical constants of Ta_2O_5 films: (**a**) refractive index and (**b**) extinction coefficient.

To study the energy band structure of the Ta_2O_5 films deposited with different ionic oxygen concentrations, the optical band gap, E_g, was determined using the Tauc mapping method[28]. The optical band gap is an important parameter for characterizing the short-wave absorption limit and evaluating film absorption. Figure 9 shows the $(\alpha h\nu)^{1/2}$ and $h\nu$ spectra of Ta_2O_5 films deposited at different APS oxygen flow rates. Compared to the films deposited with an APS oxygen flow rate of 30 sccm, the optical bandgap of the deposited films decreased from the initial value of 4.20 eV to 4.17 and 4.14 eV with APS oxygen flow rates of 25 and 35 sccm, respectively. These decreases in the optical band gap were attributed to the increase in oxygen vacancy defects and the decrease in the stoichiometric ratio of the Ta_2O_5 films[36–38]. Therefore, an appropriate ionic oxygen concentration could increase the oxidizing ability of the films, decrease the imbalance of the stoichiometric ratio, and decrease the oxygen vacancy defects in the films, which play an important role in the preparation of ultralow-absorption optical thin films.

Conclusion

Ta_2O_5 monolayers with different ionic oxygen concentrations were prepared using ion-assisted electron-beam evaporation. The effects of different ionic oxygen concentrations on the elemental content, binding energy, energy band structure, weak absorption at 1064 nm, and temperature increase of the Ta_2O_5 films were investigated. The ionic oxygen concentration affected the optical bandgap of the Ta_2O_5 films, and an appropriate ionic oxygen concentration could produce films with a larger optical bandgap. XPS tests and Ta and O elemental split-peak fitting results showed that Ta_2O_5 films deposited with an appropriate ionic oxygen concentration had fewer oxygen vacancy defects, better stoichiometric ratios, and better oxidation, resulting in less absorption and temperature rise. In addition, the link between the macroscopic absorption properties and microstructure of the Ta_2O_5 films was explained from the microstructural perspective. The primary reason for the reduced absorption loss in the Ta_2O_5 films was the appropriate ionic oxygen concentration, which improved the optical bandgap, refined the stoichiometric ratio, and reduced the oxygen vacancy defects of the films. For Ta_2O_5 monolayers deposited with an appropriate ionic oxygen concentration, the weak absorption at 1064 nm was approximately 7.2 ppm, and the temperature rise during 1064 nm continuous laser irradiation at a power density of 35 kW/cm^2 for 60 s was approximately 0.6 °C, 1/4 and 1/3 of the values for monolayers deposited with an excessive ionic oxygen concentration, respectively. This study showed that regulating the ionic oxygen concentration during the evaporative deposition of the film layer could improve the film absorption characteristics. The optimal ionic oxygen concentration was beneficial for compensating for the loss of oxygen in the film material during the evaporation process, whereas an excessively high ionic oxygen concentration increased the film layer loss. Thus, these results provide a reference for the development of ultralow absorption loss multilayer laser films for optical systems.

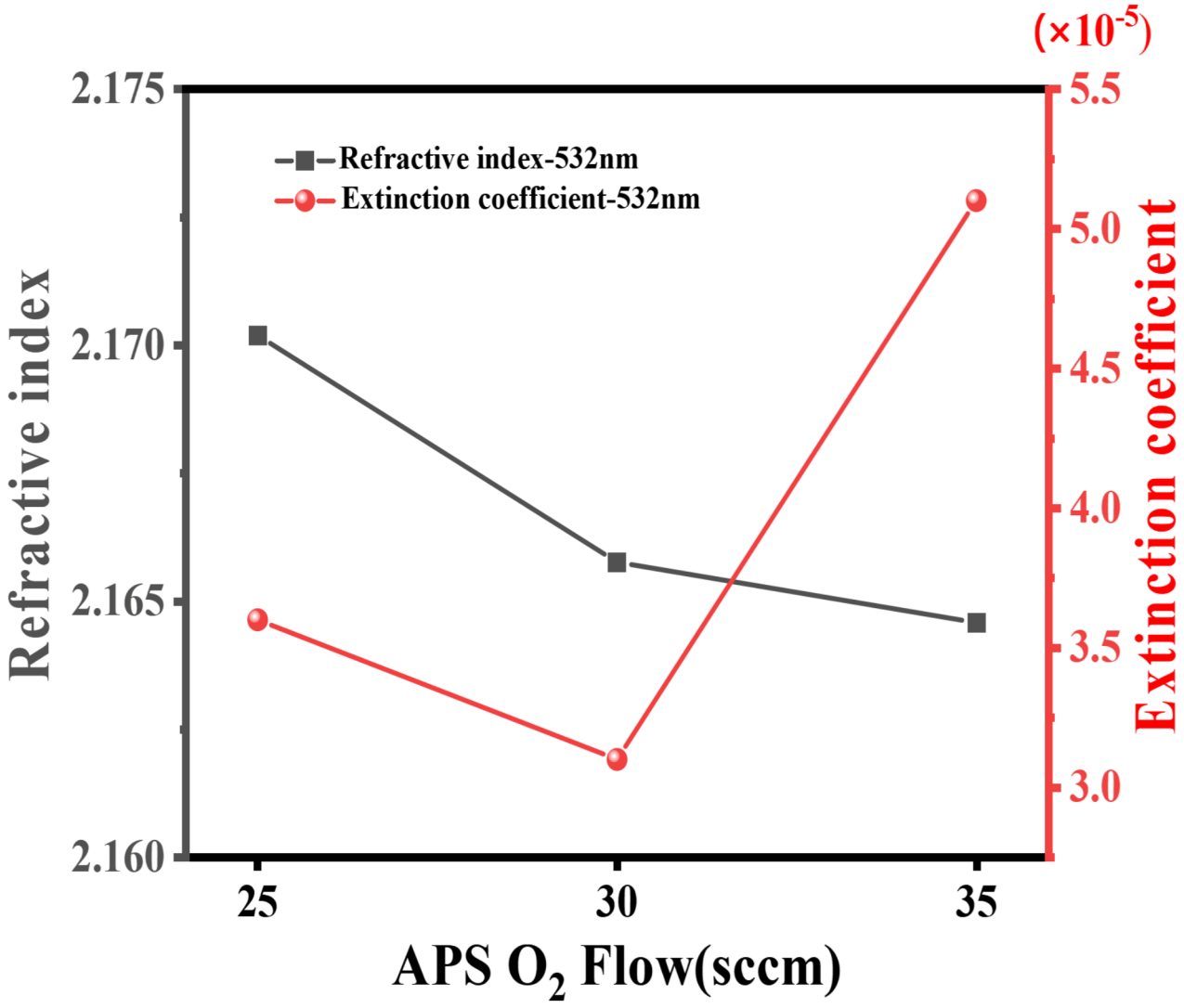

Fig. 3. Refractive index and Extinction coefficient at 532 nm of Ta_2O_5 films with different APS oxygen flow rates.

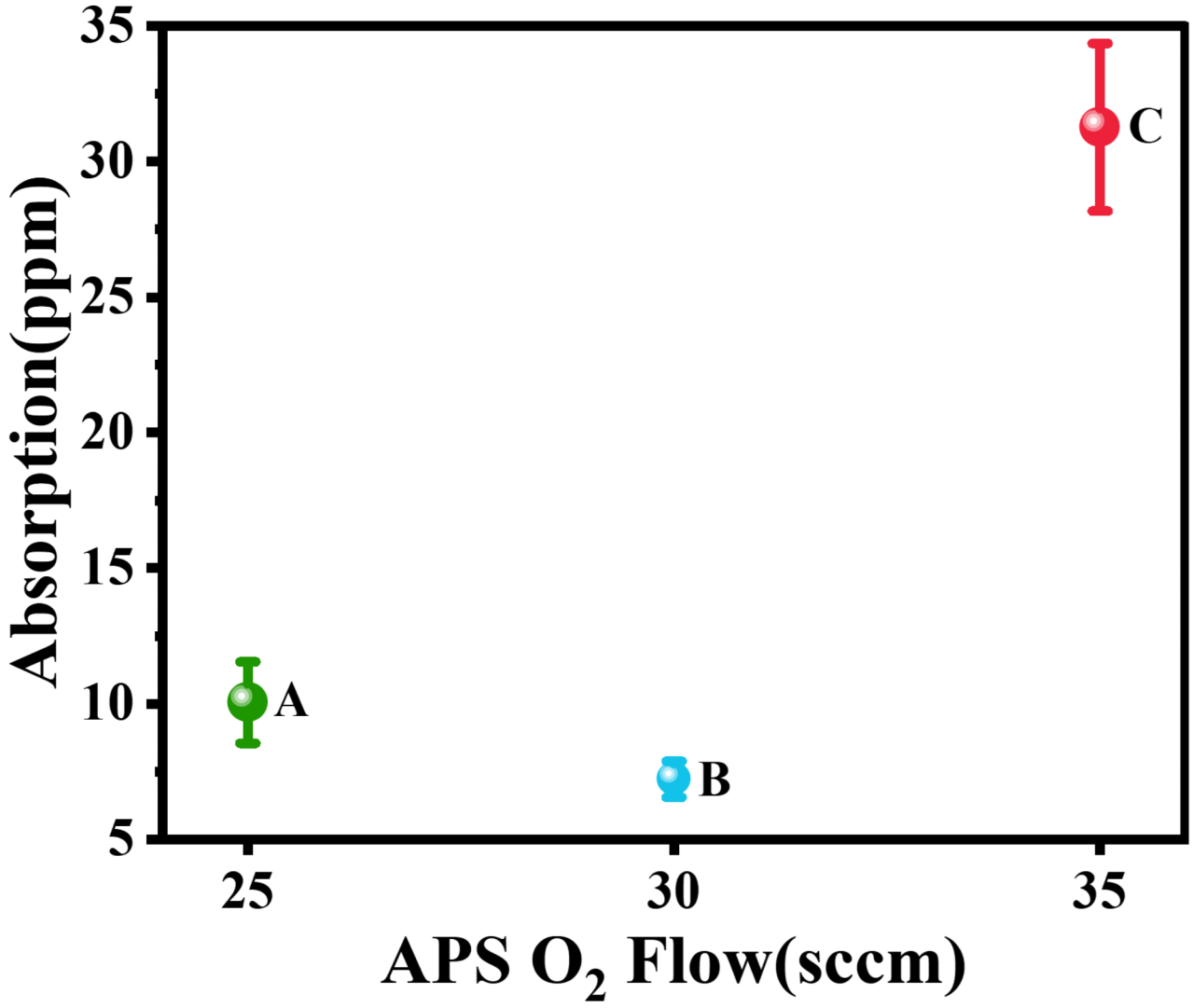

Fig. 4. Weak absorption at 1064 nm of Ta_2O_5 films with different APS oxygen flow rates.

Wavelength (nm)	Irradiation time (s)	Spot area (mm^2)	Laser power (W)	Laser power density (kW/cm^2)
1064	60	1	78	8
			157	16
			236	24
			316	32
			346	35

Table 3. Laser parameters for surface temperature rise testing.

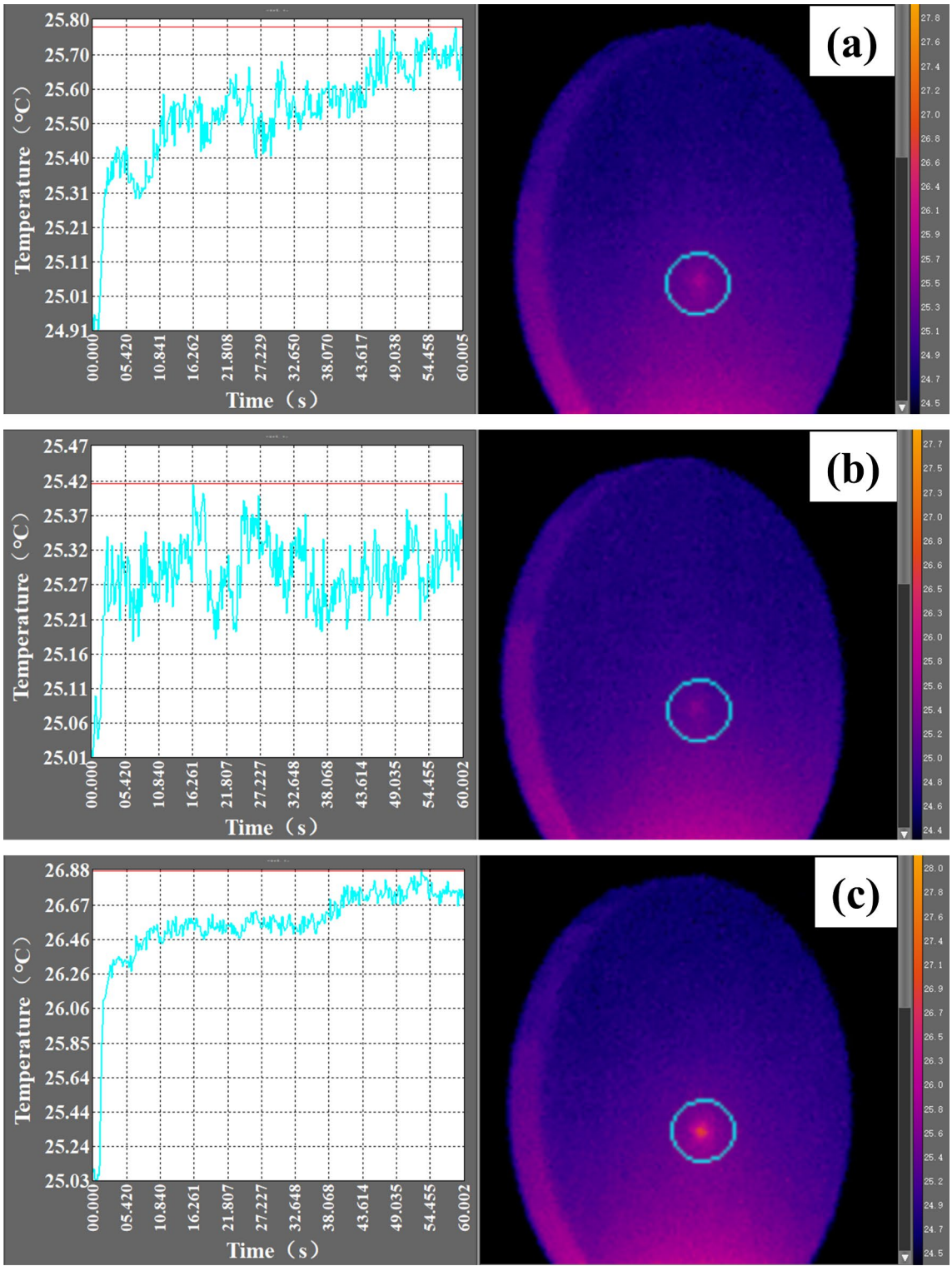

Fig. 5. Thermal camera monitoring results for the surface temperature distributions of Ta_2O_5 films with different APS oxygen flow rates: (**a**) 25, (**b**) 30, and (**c**) 35 sccm.

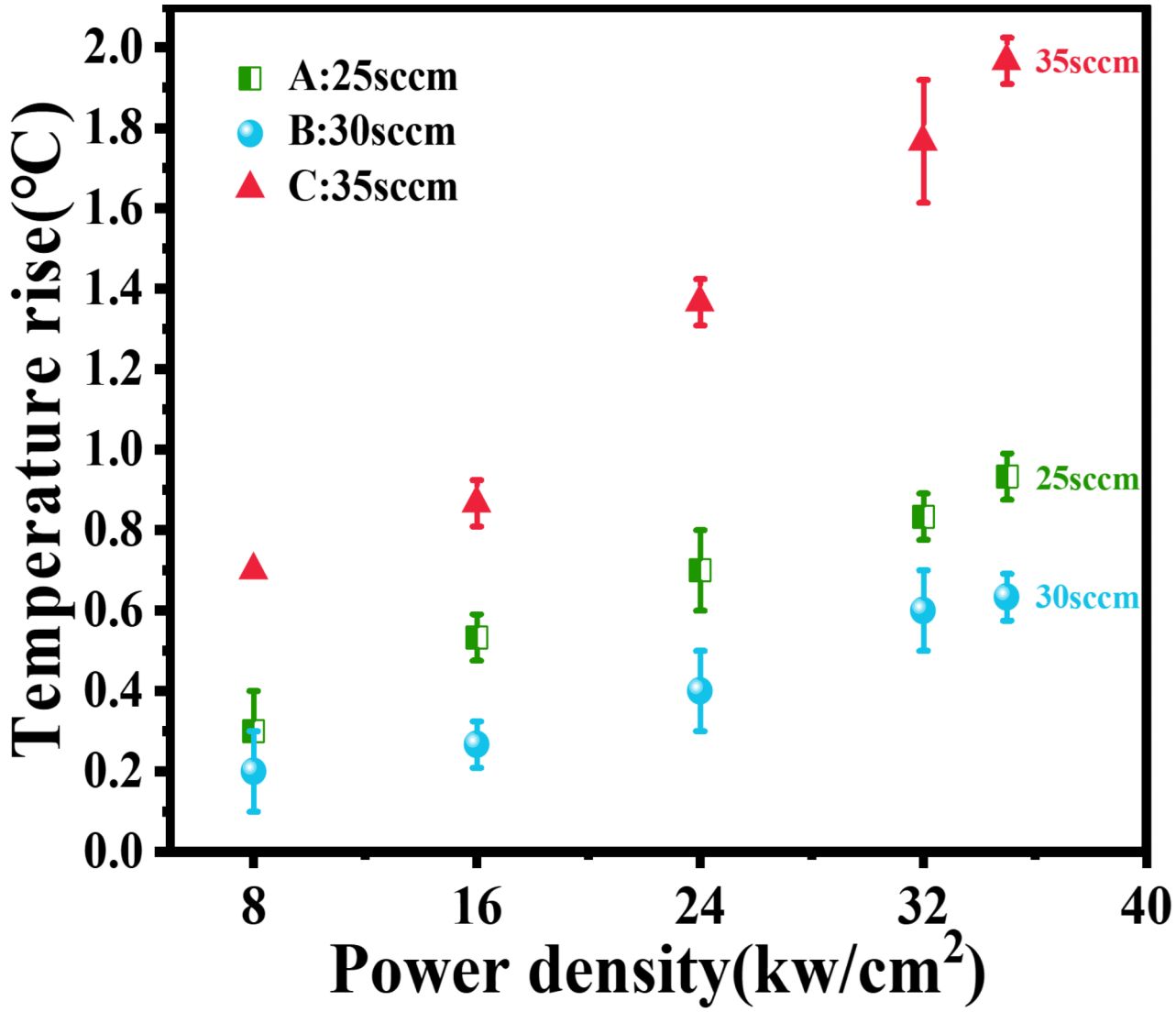

Fig. 6. Temperature rise values for samples in groups A–C at different irradiation power densities.

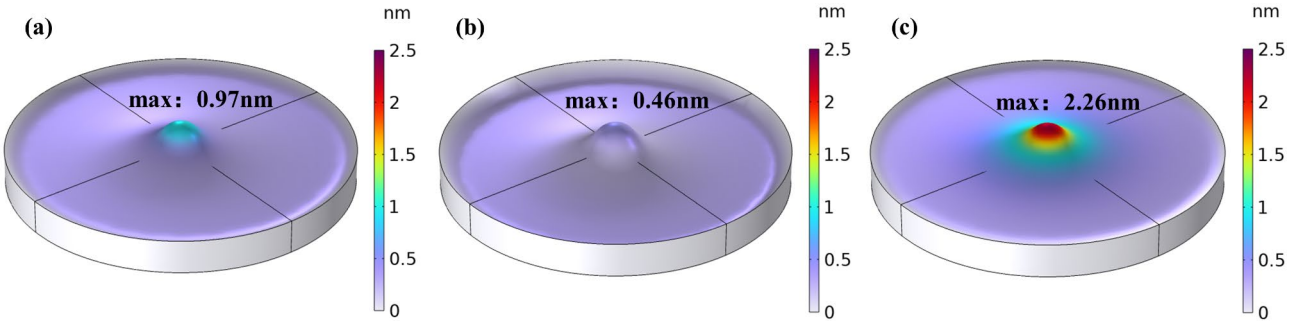

Fig. 7. COMSOL simulation results for the surface morphology distributions of Ta_2O_5 films with different APS oxygen flow rates: (**a**) 25, (**b**) 30, and (**c**) 35 sccm.

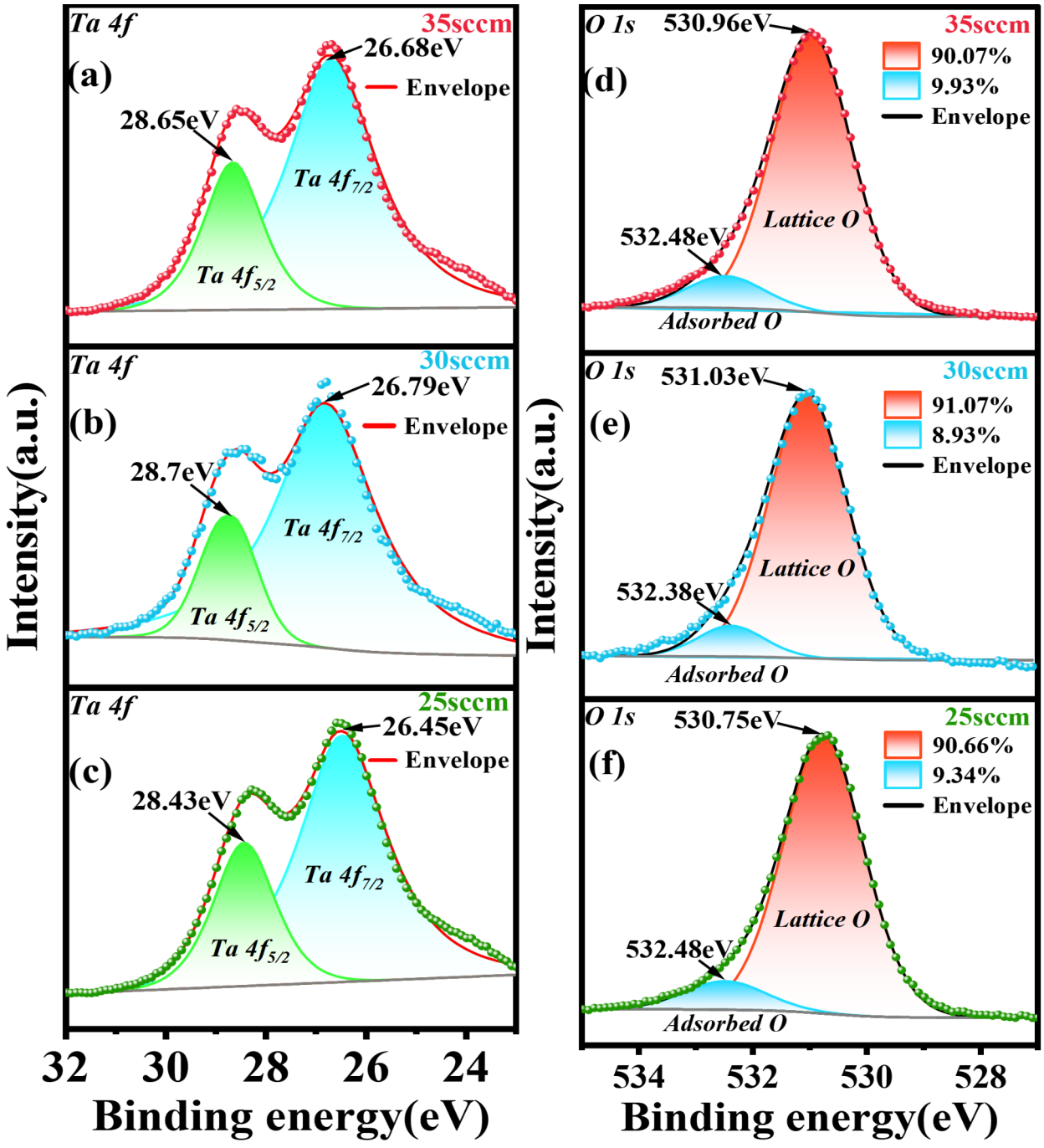

Fig. 8. (**a**–**c**) Ta 4f fine spectra; (**d**–**f**) O 1s fine spectra of Ta_2O_5 films deposited with different APS oxygen flow rates.

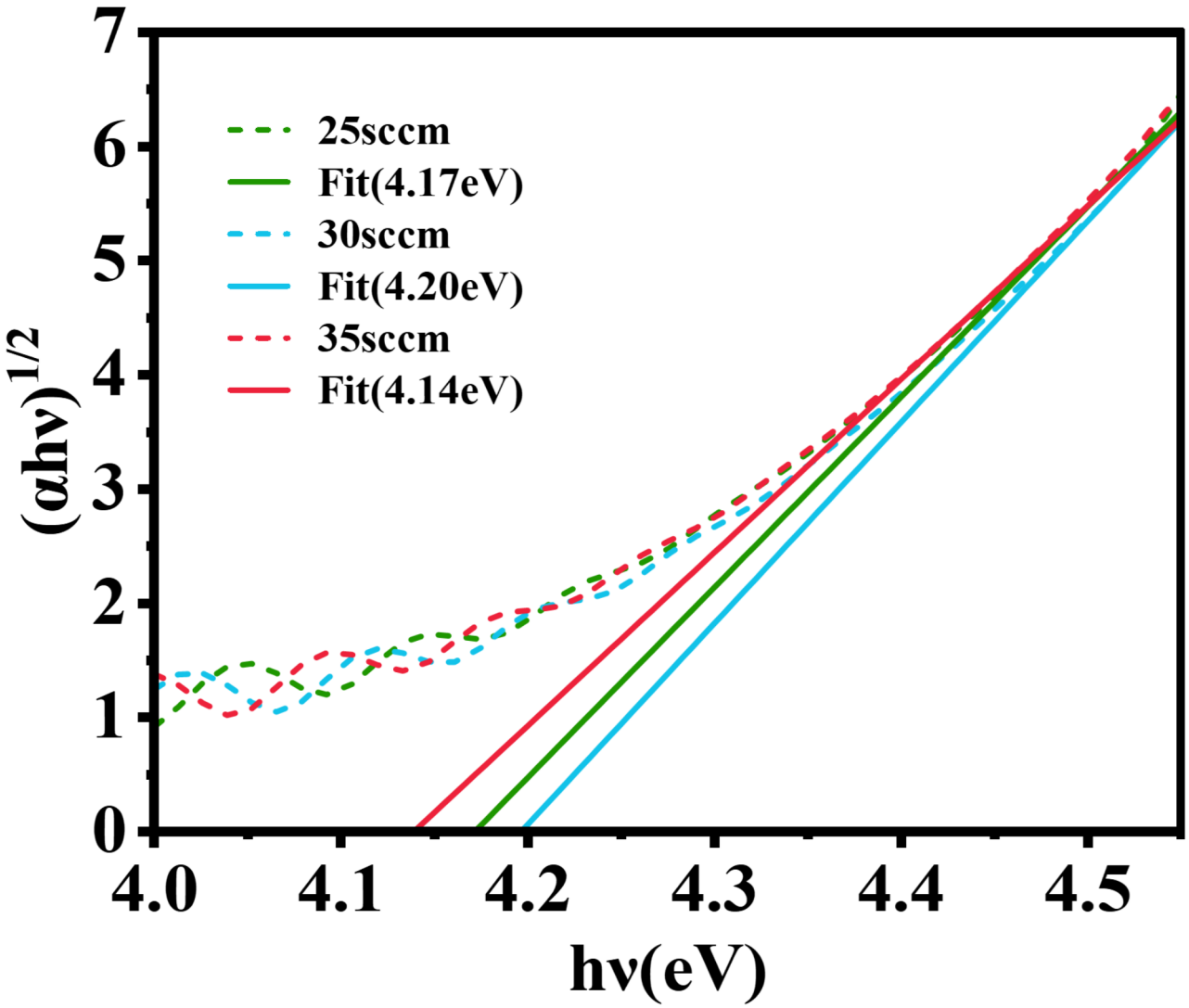

Fig. 9. Variation of $(\alpha h\nu)^{1/2}$ with photon energy for Ta_2O_5 films deposited at different APS oxygen flow rates.

Data availability

The datasets generated and/or analysed during the current study are not publicly available due to data security and privacy protection but are available from the corresponding author on reasonable request.

Received: 12 August 2024; Accepted: 8 January 2025
Published online: 03 February 2025

References

1. Cook, J. High-energy laser weapons since the early 1960s. *Opt. Eng.* **52**, 021007–021007. https://doi.org/10.1117/1.OE.52.2.021007 (2013).
2. Karr, T. & Trebes, J. The new laser weapons. *Phys. Today*. **77**, 32–38. https://doi.org/10.1063/PT.3.5380 (2024).
3. Luo, Q., Bo, F., Kong, Y., Zhang, G. & Xu, J. Advances in lithium niobate thin-film lasers and amplifiers: a review. *Adv. Photonics*. **5**, 034002–034002. https://doi.org/10.1117/1.AP.5.3.034002 (2023).
4. Aleksandrova, I., Koresheva, E. & Koshelev, E. A high-pinning-Type-II superconducting maglev for ICF target delivery: main principles, material options and demonstration models. *High. Power Laser Sci. Eng.* **10**, e11. https://doi.org/10.1017/hpl.2022.1 (2022).
5. Cristoforetti, G. et al. Multibeam laser–plasma interaction at the Gekko XII laser facility in conditions relevant for direct-drive inertial confinement fusion. *High. Power Laser Sci. Eng.* **11**, e24. https://doi.org/10.1017/hpl.2023.13 (2023).
6. Danson, C. & Gizzi, L. Inertial confinement fusion ignition achieved at the National Ignition facility–an editorial. *High. Power Laser Sci. Eng.* **11**, e40. https://doi.org/10.1017/hpl.2023.38 (2023).
7. Tao, T., Zheng, G., Jia, Q., Yan, R. & Zheng, J. Laser pulse shape designer for direct-drive inertial confinement fusion implosions. *High. Power Laser Sci. Eng.* **11**, e41. https://doi.org/10.1017/hpl.2023.35 (2023).
8. Zhang, Y. et al. Theoretical analysis of frequency modulation-to-amplitude modulation on the final optics and target of the SG II-Up laser facility. *High. Power Laser Sci. Eng.* **12**, e9. https://doi.org/10.1017/hpl.2023.89 (2024).

9. Mitrofanov, V. P. et al. Technology for the next gravitational wave detectors. *Sci. China Ser. G.* **58**, 1–26. https://doi.org/10.1007/s11433-015-5738-8 (2015).
10. Granata, M. et al. Amorphous optical coatings of present gravitational-wave interferometers. *Classical Quantum Gravity*. **37**, 095004. https://doi.org/10.1088/1361-6382/ab77e9 (2020).
11. Wang, G. et al. Analysis and suppression of thermal effect of an ultra-stable laser interferometer for space-based gravitational waves detection. *Chin. Opt. Lett.* **20**, 011203. https://doi.org/10.3788/COL202220.011203 (2022).
12. Sanders, V. High-precision reflectivity measurement technique for low-loss laser mirrors. *Appl. Opt.* **16**, 19–20. https://doi.org/10.1364/AO.16.000019 (1977).
13. Gao, C., Gaur, P., Rubin, S. & Fainman, Y. Thin liquid film as an optical nonlinear-nonlocal medium and memory element in integrated optofluidic reservoir computer. *Adv. Photonics*. **4**, 046005–046005. https://doi.org/10.1117/1.AP.4.4.046005 (2022).
14. Park, K., Lee, D., Kim, K. & Moon, D. Growth and characterization of Ta_2O_5 thin films on Si by ion beam sputter deposition. *Thin Solid Films*. **281**, 419–422. https://doi.org/10.1016/0040-6090(96)08666-X (1996).
15. Vazimali, M. G. & Fathpour, S. Applications of thin-film lithium niobate in nonlinear integrated photonics. *Adv. Photonics*. **4**, 034001–034001. https://doi.org/10.1117/1.AP.4.3.034001 (2022).
16. Todorova, Z. et al. Electrical and optical characteristics of Ta_2O_5 Thin films deposited by Electron-Beam Vapor Deposition. *Plasma Processes Polym.* **3**, 174–178. https://doi.org/10.1002/ppap.200500110 (2006).
17. Farhan, M. S., Zalnezhad, E. & Bushroa, A. Properties of Ta_2O_5 thin films prepared by ion-assisted deposition. *Mater. Res. Bull.* **48**, 4206–4209. https://doi.org/10.1016/j.materresbull.2013.06.068 (2013).
18. Xu, C. et al. Correlations between the oxygen deficiency and the laser damage resistance of different oxide films. *Appl. Surf. Sci.* **289**, 141–144. https://doi.org/10.1016/j.apsusc.2013.10.121 (2014).
19. Cosar, M., Ozhan, A. & Aydogdu, G. Improving the laser damage resistance of oxide thin films and multilayers via tailoring ion beam sputtering parameters. *Appl. Surf. Sci.* **336**, 34–38. https://doi.org/10.1016/j.apsusc.2014.09.048 (2015).
20. Shuai, K. et al. Multilayer dielectric grating pillar-removal damage induced by a picosecond laser. *High. Power Laser Sci. Eng.* **10**, e42. https://doi.org/10.1017/hpl.2022.34 (2022).
21. Zhang, G., Xue, Y. & Guo, P. Research on the Ta_2O_5 optical thin films deposited by electron beam evaporation with ion assisted. *Piezoelectectrics Acoustooptics*. **30**, 12–15 (2008).
22. Liu, H. et al. Characteristics of optical band gap of tantalum oxide thin film deposited by ion beam sputtering. *Opt. Precision Eng.* **25**, 21–27 (2017).
23. Chen, C. et al. Effect of ionic oxygen concentration on properties of SiO_2 and Ta_2O_5 monolayers deposited by ion beam sputtering. *Opt. Mater.* **136**, 113349. https://doi.org/10.1016/j.optmat.2022.113349 (2023).
24. Essential Macleod. https://www.thinfilmcenter.com/
25. Manifacier, J., Gasiot, J. & Fillard, J. A simple method for the determination of the optical constants n, k and the thickness of a weakly absorbing thin film. *J. Phys. E: Sci. Instrum.* **9**, 1002. https://doi.org/10.1088/0022-3735/9/11/032 (1976).
26. Chow, R., Taylor, J. R. & Wu, Z. L. Absorptance behavior of optical coatings for high-average-power laser applications. *Appl. Opt.* **39**, 650–658. https://doi.org/10.1364/AO.39.000650/ (2000).
27. Fan, S., He, H., Shao, J., Fan, Z. & Zhang, D. in *Fifth International Conference on Thin Film Physics and Applications*. 531–534 (SPIE).
28. Tauc, J., Grigorovici, R. & Vancu, A. Optical properties and electronic structure of amorphous germanium. *Phys. Status Solidi B.* **15**, 627–637. https://doi.org/10.1002/pssb.19660150224 (1966).
29. Ren, W. et al. Annealing effects on the optical and electrochemical properties of tantalum pentoxide films. *J. Adv. Ceram.* **10**, 704–713. https://doi.org/10.1007/s40145-021-0465-2 (2021).
30. COMSOL Multiphysics. https://www.cn.comsol.com/
31. Szymanowski, H., Zabeida, O., Klemberg-Sapieha, J. & Martinu, L. Optical properties and microstructure of plasma deposited Ta_2O_5 and Nb_2O_5 films. *J. Vac Sci. Technol. A.* **23**, 241–247. https://doi.org/10.1116/1.1851544 (2005).
32. Korkos, S. et al. XPS analysis and electrical conduction mechanisms of atomic layer deposition grown Ta_2O_5 thin films onto p-Si substrates. *J. Vac Sci. Technol. A.* **38** https://doi.org/10.1116/1.5134764 (2020).
33. Mannequin, C., Tsuruoka, T., Hasegawa, T. & Aono, M. Identification and roles of nonstoichiometric oxygen in amorphous Ta_2O_5 thin films deposited by electron beam and sputtering processes. *Appl. Surf. Sci.* **385**, 426–435. https://doi.org/10.1016/j.apsusc.2016.04.099 (2016).
34. Tsuchiya, T. et al. X-ray absorption, photoemission spectroscopy, and Raman scattering analysis of amorphous tantalum oxide with a large extent of oxygen nonstoichiometry. *Phys. Chem. Chem. Phys.* **13**, 17013–17018. https://doi.org/10.1039/C1CP21310E (2011).
35. Brumbach, M. T. et al. Evaluating tantalum oxide stoichiometry and oxidation states for optimal memristor performance. *J. Vac Sci. Technol. A.* **32** https://doi.org/10.1116/1.4893929 (2014).
36. Briand, D. et al. Metallo-organic low-pressure chemical vapor deposition of Ta_2O_5 using TaC12H30O5N as precursor for batch fabrication of microsystems. *Thin Solid Films*. **493**, 6–12. https://doi.org/10.1016/j.tsf.2005.03.021 (2005).
37. Xu, C. et al. Effect of oxygen vacancy on the band gap and nanosecond laser-induced damage threshold of Ta_2O_5 films. *Chin. Phys. Lett.* **29**, 084207. https://doi.org/10.1088/0256-307X/29/8/084207 (2012).
38. Wang, L. et al. Effects of hot-isostatic pressing and annealing post-treatment on HfO_2 and Ta_2O_5 films prepared by ion beam sputtering. *Optik* **142**, 33–41. https://doi.org/10.1016/j.ijleo.2017.05.047 (2017).

Author contributions

Lin Wang: Investigation, Data curation, Writing - original draft. Weili Zhang: Supervision. Ruijin Hong: Supervision. Kun Wang: Formal analysis. Menglei Wang: Software. Qinmin Wang: Data curation. Kui Yi: Project administration, Validation. Jianda Shao: Funding acquisition.

Declarations

Competing interests

The authors declare no competing interests.

Additional information

Correspondence and requests for materials should be addressed to W.Z. or R.H.

Reprints and permissions information is available at www.nature.com/reprints.

Publisher's note Springer Nature remains neutral with regard to jurisdictional claims in published maps and institutional affiliations.